Hydrol. Earth Syst. Sci. Discuss., 5, 3129–3156, 2008
www.hydrol-earth-syst-sci-discuss.net/5/3129/2008/

Hydrology and Earth System Sciences Discussions

Papers published in *Hydrology and Earth System Sciences Discussions* are under open-access review for the journal *Hydrology and Earth System Sciences*

Assessing snow water equivalent of an Alpine catchment using snow dynamic model calibrated with satellite images

C. Corbari[1], **G. Ravazzani**[1], **J. Martinelli**[2], **and M. Mancini**[1]

[1]Politecnico of Milan, Milan, Italy
[2]Pirelli Ambiente Site Remediation, Milan, Italy

Received: 18 September 2008 – Accepted: 22 September 2008
– Published: 14 November 2008

Correspondence to: C. Corbari (chiara.corbari@mail.polimi.it)

Published by Copernicus Publications on behalf of the European Geosciences Union.

Abstract

This paper presents a simplified numerical model of snow dynamic implemented into a continuous distributed hydrological model for hydrograph simulations at basin scale. This snow model is based on air temperature thresholds that rule the snow melt and accumulation processes.

A procedure to calibrate these temperature thresholds from NOAA satellite snow cover maps is discussed. We show that, for an accurate model calibration from satellite images, it is necessary to consider the presence of areas with complex topography such as mountain slopes.

Snow model performance is tested both at local and basin scale on Alpine catchment. At local scale a good agreement between modelled snow dynamic and observed snow height data at snow gauge stations in the river Anza basin (Italy) is shown; at basin scale agreement between observed and simulated hydrographs at the discharge station of river Toce (Italy) is reported.

1 Introduction

The snow dynamic and its spatial variability act as a "large mountain" reservoir due to the shift in time of the water volume determining the flow regime in the rivers network. Its role is well known to be very important on the river flow hydrograph for low as well as for high discharge regimes. For this reason and for its operative impact on the management of water resources in mountain basins, a considerable amount of research effort leading to several major improvements in the modelling technique has been done (Verbunt et al., 2003; Huwald et al., 2006; Shamir et al.,2006).

Despite the important role played by the snow and despite the capability reached by the scientific and technical community to model its dynamic, one of the main uncertainties lies in the determination of the snow covered areas and of their water equivalent. This is due to the well known difficulties of monitoring snow parameters and of de-

HESSD

5, 3129–3156, 2008

tecting the snow coverage on areas of complex topography such as mountain slopes (Bocchiola and Rosso, 2007). Nowadays, the potentiality of images from remote sensing is well assessed by the scientific community (Baumgartner et al., 1994; Metsiimiiki et al., 1998, Parajka and Bloschl, 2008), but the conversion from qualitative data to quantitative ones is still very complex. This is due to the spatial and radiometric integration underlined in the pixel value of digital number given for any satellite image. This problem is evident in several fields of land observation.

Several methodologies have been considered to improve the use of satellite images ranging from the field of numerical modelling and ground measurements of snow parameters (Dressler et al., 2006; Bitner et al., 2002; Lee et al., 2005; Ranzi et al., 1999; Tachner et al., 1998) to the development of empirical relationships between flow discharge and snow accumulation and melt (Martinec, 1991).

This work proposes the use of NOAA AVHRR (Advanced Very High Resolution Radiometer) satellite images (NOAA, 2000) to calibrate a distributed model, based on air temperature thresholds (Salandin et al., 2004), for the simulation of snow dynamic on alpine watersheds. Snow coverage retrieved from satellite images needs to be corrected to remove the gaps due to the presence of shaded area.

The proposed methodology is validated at local scale by comparison of modelled and measured snow depth evolution. However this approach gives only a qualitative verification of the timing of the snow dynamic because snow gauges do not provide information on the snow water equivalent. This methodology is also validated at basin scale where a good agreement between observed and simulated hydrographs at the discharge station of river Toce (Italy) is observed.

2 The Anza river basin

The Anza river basin is a typical alpine basin with a total drainage area of about 261 km^2, with nearly 37% of the total area above 2000 m a.s.l. It is located in the north of the Piedmont region in Italy and in the Toce basin (Fig. 1).

Climate conditions are typically humid, characterized by higher precipitations in autumn and spring. The annual average precipitation on the Toce watershed is, with its more than 2000 mm, the highest value of the whole River Po basin. Climatic characteristics, together with morphology and soil texture, frequently induced flood events in the past years.

2.1 Physiographic basin characterization

Available digital cartographic data include: the Digital Elevation Model (DEM) available in raster format at 100 m×100 m resolution; CORINE land cover maps (CEC, 1994; EEA, 2000) updated in the year 2000 available in vector format; pedologic characteristics for soils available in vector format. From the available basic thematic layers, basin parameters required for the application of the hydrological model have been derived at a spatial resolution of 500 m×500 m. These include: curve number (Soil Conservation Service, 1986), flow direction, slope and aspect, residual and saturated soil moisture, albedo, pore size distribution index, saturated hydraulic conductivity, wilting point, field capacity and soil depth.

2.2 Hydrologic and meteorological data

For this study, meteorological and hydrologic measured ground data were collected by the telemetric monitoring system of the Regione Piemonte. Rainfall, air temperature, incident short wave solar radiation and air relative humidity data are available from 1 January 2000 to 31 December 2004 at hourly or sub-hourly time interval. The locations of the 25 available rain gauges and the 25 thermometers for air temperature measurements at 2 m above the ground are shown in Fig. 1 for the whole Toce basin. Hydrometric observations at 30 min time step at the Anza basin outlet, Piedimulera (Fig. 1), and at the Toce basin outlet, Candoglia, are available from 1 January 2000 to 31 December 2003.

HESSD
5, 3129–3156, 2008

2.3 Snow data: satellite images and ground measurements

The satellite images used to retrieve snow coverage are taken by the polar satellites NOAA-AVHRR (Advanced Very High Resolution Radiometer). The AVHRR (NOAA, 2000) is a six channel radiometer that detects energy in the visible and infrared spectral bands. These images are characterized by a nominal spatial resolution of 1.1 km at nadir. The images are updated by a new passage of the satellite twice a day, one in daytime and the other after the sunset. However for this study only daytime images were considered.

For the four years studied, up to 21 images referring both to the accumulation period and, most frequently, to the melting period were collected. Since in the visible band reflectivity of cloud and snow is very similar (Henderson and Sellers, 1984) it is difficult to distinguish between them. Therefore, only images without clouds were used.

Ground measurements of snow height are given by 1 snow gauge located in the river Anza basin at an elevation over 2000 m a.s.l. and by other 6 snow gauges in the whole river Toce basin; these data are available every 30 min for the period 2000–2003.

3 Snow cover classification from satellite for complex topography

Snow covered pixels were classified with a supervised approach from the visible band. In fact, snow is easily classified from satellites images for clear sky conditions, due to the high reflectivity of the snow in the visible band. In fact, in this spectral band snow has higher values than all the others type of ground covers (Choudhury, 1979).

However some anomalies were encountered, in area with no return signal, mostly where the surface was covered by a mixture of exposed soil and snow, over densely forested areas (Voigt et al., 1999) and also in those pixels affected by shadow (Simpson et al., 1998; Baral and Gupta, 1997). Consequently, it was frequently noted that area usually covered by snow were classified as snow free pixels.

Influence of shadow on pixel classification is shown in Fig. 4. A zoom of the entire

HESSD
5, 3129–3156, 2008

basin is presented. It is characterized by very high elevations. Digital elevation model was resampled at the same spatial resolution of NOAA images (1100 m). A map of shadowed pixels was produced, related to the time when the satellite image was taken. A module taking into account the shadow effect induced by topography was developed. The algorithm calculates the angle, Ψ, between the point, denoted by coordinate x_m, y_m, z_m, with maximum elevation in the direction of the solar beam, and the examined cell, denoted by coordinated x_0, y_0, z_0 (Fig. 3):

$$\psi = arctg\left[(z_m - z_o)/\sqrt{(x_m - x_o)^2 + (y_m - y_o)^2}\right] \quad (1)$$

If Ψ is higher then the sun elevation, the cell is shadowed.

The corrected image was compared to the snow coverage retrieved from pixel classification and a strong correlation is shown between shadowed pixels and pixels falsely classified as not covered by snow. In order to reduce this error, an elevation based correction was applied. According to this method all pixels above a reference altitude were considered as snow covered. Reference altitude is fixed as the mean altitude of snow on the satellite image. The basic assumption is that if a pixel is classified as not covered but, in the nearby, a covered pixel at lower elevation exists, a correction is applied.

In Table 1 the percentage of snow covered pixels from row satellite images (second column) and after elevation correction (third column) is reported.

4 The snow dynamic model

4.1 The snow model

The snow model computes snow melt and snow accumulation dynamics. This module is included into a continuous distributed hydrological water-balance model, FEST-WB (Mancini, 1990; Montaldo et al., 2007, Rabuffetti et al., 2008).

HESSD
5, 3129–3156, 2008

The partitioning of the total precipitation, P, in liquid, P_l, and solid, P_s, phase is a function of the air temperature, Ta (Tarboton et al., 1994):

$$P_l = \alpha_P P \tag{2a}$$

$$P_s = (1 - \alpha_P) P \tag{2b}$$

where $\alpha_P$is computed by:

$$\begin{cases} \alpha_P = 0 & \text{if} \quad T_a \le T_{\text{low}} \\ \alpha_P = 1 & \text{if} \quad T_a \ge T_{\text{up}} \\ \alpha_P = \frac{T_a - T_{\text{low}}}{T_{\text{up}} - T_{\text{low}}} & \text{if} \quad T_{\text{low}} \le T_a \le T_{\text{up}} \end{cases} \tag{3}$$

where T_{low} and T_{up} are calibrating parameters.

The snow melt simulation is based on the degree day concept (Martinec et al., 1960; Hock, 2003). The melt rate in m/s, M_s, is proportional to the difference between air temperature and a predefined threshold temperature, T_b:

$$M_s = C_m (T_a - T_b) \tag{4}$$

where C_m ($\mathrm{m\,^{\circ}C^{-1}\,s^{-1}}$) is an empirical coefficient depending on meteorological conditions and geographic location.

Spatial distribution of air temperature local measurements have to consider the reduction of temperature with altitude. In the model a constant lapse rate adjusts temperature for elevation ($-0.0065\,^{\circ}\mathrm{C\,m^{-1}}$). Thermal inversion phenomena are neglected.

The terrain covered by snow is supposed to be frozen, and hence the melted water is prevented from infiltrating into the soil. On the contrary, the liquid fraction of snow water equivalent, R_s, sum of melted water and liquid precipitation, is supposed to flow cell by cell trough the snow pack with a linear reservoir routing scheme (Ponce, 1989) with a celerity of 1.67×10^{-3} m/s (Salandin et al., 2004; Verbunt et al., 2003). When R_s reaches a cell not covered by snow, it is added to the liquid precipitation of that cell.

HESSD
5, 3129–3156, 2008

4.2 Calibration from satellite images

The calibration of snow accumulation temperature parameters, T_{low} and T_{up}, in Eq. (3), is based on the comparison of simulated snow cover extent with the one retrieved from satellite images.

The threshold temperature values depend on local meteorological conditions, so a wide range of values has been used in literature, from -1°C to 3°C (Tarboton et al., 1996), from -1°C to 7°C (Braun, 1991), from 0.5°C to 1°C (US Army Corps of Engineers, 1956) and Martinec and Rango (1986) referred to maximum values as 5.5.

The two threshold temperatures were changed in the range $7^{\circ}\text{C} \div -5^{\circ}$C with a "trial and error" approach, having as target the minimization of the root mean square error (RMSE) and the maximization of the efficiency of Nash and Sutcliffe (1970) defined as

$$\eta = 1 - \frac{\sum_{j=1}^{n_t} \left(N_{m,j} - N_{o,j}\right)^2}{\sum_{j=1}^{n_t} \left(N_{o,j} - \overline{N_o}\right)^2} \quad (5)$$

where n_t is the total number of maps, $N_{o,j}$ and $N_{m,j}$ are the observed and modeled number of snow covered pixels for map j, respectively, and $\overline{N_o}$ is the mean of the observed number of snow covered pixels.

The snow melt parameters, T_b and C_m in Eq. (4), are assumed to be, respectively, 0°C and 5.5 10^{-8} m $^{\circ}\text{C}^{-1}$ s^{-1} (Salandin et al., 2004).

The calibration of the other parameters of the distributed model is reported in Rabuffetti et al. (2008).

The calibration period is from 1 August 2000 till 1 June 2002, while the validation period goes from 1 August 2002 till 31 December 2003.

The results of the calibration based on raw satellite images are summarised in Fig. 5, where the number of snow covered pixels retrieved from satellite images is plotted

HESSD
5, 3129–3156, 2008

against the number of snow covered pixels simulated by the distributed model for different combination of T_{low} and T_{up}. We note (Table 2) that the values of calibrating parameters that maximise the Nash and Sutcliffe efficiency and minimize the RMSE are −3°C for T_{low} and 0°C for T_{up}, thus exceeding the range accepted by literature.

The results of the calibration based on the proposed correction procedure for satellite images are summarised in Fig. 6a. The values of best fit calibrating parameters (Table 2) are 0°C for T_{low} and 0°C for T_{up}, in the range accepted by literature.

5 The model results

5.1 Snow cover maps from satellite and modelling simulation

The validation period goes from 1 August 2002 till 31 December 2003 where a comparison between the snow cover maps from corrected satellite images and the simulated snow cover areas is made. For the modelling simulation only the calibration temperature thresholds, 0°C for T_{low} and 0°C for T_{up}, are used.

In Fig. 6b the number of snow cover pixels of the corrected satellite images and of the simulated maps for the given temperature thresholds are reported and good results are obtained with the Nash and Sutcliffe efficiency of 0.21 and a RMSE of 30 pixels.

5.2 Simulated snow dynamic and ground measurements

The snow model and the methodology for its calibration are also validated at local scale by comparing simulated and observed data. The output of the implemented snow model is the snow pack water equivalent; however, ground measurements are expressed in real height. Therefore direct comparison of simulated and observed heights is possible only if the snow density is known. Unfortunately, snow density is very changeable (Diamond e Lowry, 1953) and hence difficult to be estimated; in fact after falling, snow tends to increase its density and at the same time to decrease its

height due to compression under its own weight and to continuous structural changes. In fact the snow density can be approximated to 100 kg m^{-3} for fresh snow, but it can increase four or five times up to values between 400 and 500 kg m^{-3} with time.

The measured height of the snow pack and the modelled snow water equivalent are normalized dividing by their respective maximum values, thus avoiding the problem of comparison.

In Fig. 7 comparison of the temporal dynamic of normalized snow depth is reported for Macugnaga station in the Anza basin as example. Five combination of T_{low} and T_{up} are reported: T_{low}=−1 and T_{up}=3, T_{low} = T_{up}=0, T_{low}=1 and T_{up}=7, T_{low}=−5 and T_{up}=−2 and T_{low}=−3 and T_{up}=0. Due to the lack of other station in the Anza river basin, the results for the same five combination of temperature thresholds for the Antrona Lago station, in the Toce basin, are also reported.

Simulated and observed snow data are then transformed in binary data: when snow height is greater than zero the time step is marked as "snow" while, when height is zero the time step is marked as "no-snow".

From the "snow"–"no snow" binary series it is possible to build up a contingency table (Mason and Graham, 1999) comparing the observed and the simulated data for different combination of Tup and Tlow. The contingency tables are a means to assess the ability of the model to correctly catch the temporal dynamic of the snow. Defining a hit when there is a perfect agreement between the observed ground cover condition (snowed or no snowed) and the simulated one, the performance of the model may be expressed in terms of correct performance index (CPI) (Ravazzani et al., 2007), defined as the ratio between the number of hits and the total number of time steps.

In Fig. 8 contingency tables for five combinations of T_{low} and T_{up} are reported for the studied stations. For Macugnaga station the combination of temperatures that better represents ground cover condition is T_{low} = T_{up}=0°C (CPI=86.2%), with only 202 discrepant days on a total of 1458, confirming the results obtained form the calibration with satellite images of previous paragraph. The other four combination of temperatures, T_{up}=3°C and T_{low}=−1°C and T_{up}=−2°C and T_{low}=−5°C, denote CPI of, respec-

HESSD
5, 3129–3156, 2008

tively, 83.1% and 85.4%. For T_{up}=0°C and T_{low}=−3°C CPI is equal to 83.7%, while for T_{up}=7°C and T_{low}=1°C CPI is 78.5%. The same results are found for Antrona Lago station with CPI = 89% for T_{low}=T_{up}=0°C.

5.3 Simulated and observed runoff volume

For the hydrograph simulations, the complete distributed hydrological model FEST-WB was used; it computes the main processes of the hydrological cycle such as evapotranspiration, infiltration, surface runoff, flow routing, subsurface flow and snow dynamics (Fig. 2). The computation domain is discretized with a mesh of regular square cells, within which water fluxes are calculated.

The flow in alpine basins is mainly influenced by the melt of glacier and snow and by its accumulation, as well as by the meteorological conditions and soil characteristics. In fact during winter most precipitations are cumulated as snow, while on the contrary during the melt months snow is the major contributor to rivers runoff. So this flow in alpine regions is characterized by very strong daily and seasonal fluctuations (Gurtz et al., 2002).

The results achieved with our model confirm the importance of studying the snow cycle; in fact the difference between the simulated discharge with various air temperature thresholds is evident. Melt contribution is very important both for cumulated volumes and for peaks discharge. These values are extremely variable because they strictly depend on the particular climatic conditions of each period and on basin topographic conditions.

The effect of snow dynamic on discharge simulation is shown in Fig. 9. The graphs refer to a flood event period occurred in November 2002 at the cross-section of Piedimulera. In the graphs five series are compared: discharge simulated by means of the complete hydrological model with five different combination of temperature thresholds for snow accumulation. Data are extracted from the continuous simulation for the period 2000–2003. We see that the complete hydrological model with snow accumulation thresholds of −5°C for T_{low} and −2°C for T_{up} simulated the major volume and the

highest peak of discharge; this is due correctly to the few snow accumulation. On the contrary the hydrological simulation with air temperature thresholds of 1°C for T_{low} and 7°C for T_{up} induced an elevate snow accumulation and consequentially the lowest peak of discharge and the lowest cumulated volume.

Moreover, due to the lack of reliable measured discharges at the Anza river outlet, comparison between the observed and simulated discharges is done at the control cross section of Candoglia in the Toce basin, where the Anza river is an effluent (Fig. 1).

In Fig. 10 the observed cumulated volume and the simulated one for the better accumulation temperature thresholds, T_{low}=T_{up}=0, are shown at Candoglia from 1 August 2000 till 31 December 2003 and small differences are present. Precisely the volume with this set of temperature is 8.2% underestimated compared with the observed one, but the precision is higher till 31 December 2002 where the simulated volume underestimated the observed one of only 3%. This problem is due to the fact the 2003 was a drought year where dam discharges play an important role. Snow depth was set to 0 as initial condition all over the basin at 1 January 2000; for this reason the first accumulation – melting period of the simulation was considered as a spin-up period.

6 Conclusions

The paper present two major conclusions. The first regards a procedure to correct NOAA-AVHRR satellite images respect to shadowed pixels induced from high crest in mountain areas. The correction consists in computing the shadow areas on a DEM base and than correct them assigning snow coverage according to the mean snow line elevation. Results show the relevant role that these areas can play in the estimation of snow water equivalent for Alpine catchments.

The second conclusion confirms the good performance of a distributed simplified snow dynamic model that is calibrated from corrected satellite snow images for two winter seasons and validated on different satellite snow images and snow height ground measurements.

Acknowledgements. This work was supported by the CAVE Project, funded by Fondazione Cariplo, aiming at the investigation of the potential of water stored in quarries for the maintenance of supplies in times of water scarcity. The work is also supported by Italian Ministry of University and Scientific Research (2006), project "Assimilation of remote sensing and ground data for the calibration of distributed hydrologic models and flash flood forecasting". The authors thank the ARPA Regione Piemonte (Italy), ARPA Regione Lombardia (Italy), Ufficio Federale dell'Ambiente UFAM Berna (Switzerland), Ufficio Federale di Meteorologia e Climatologia MeteoSvizzera (Switzerland) for providing the data used in the case studied.

References

Baral, D. J. and Gupta, R. P.: Integration of satellite sensor data with DEM for the study of the snow cover distribution and depletion pattern, Int. J. Remote Sens., 18, 3889–3894, 1997.

Baumgartner, M. F., Apfl, G., and Holzer, T.: Monitoring alpine snow cover variations using NOAA-AVHRR data, Geoscience and remote sensing symposium proceedings, IGRASS'94, 4, 2087–2089, doi:10.1109/IGRASS.1994.399661, 1994.

Bitner, D., Carroll, T., Cline, D., and Romanov, R.: An assessment of the differences between three satellite snow cover mapping techniques, Hydrol. Process., 16, 3723–3733, 2000.

Bocchiola, D. and Rosso, R.: The distribution of daily snow water equivalent in the central Italian Alps, Adv. Water Resour. 30, 135–147, 2007.

Braun, L. N.: Modeling the snow-water equivalent in the mountain environment, IAHS Publ., 205, 3–17, 1991.

CEC: CORINE land cover. Technical guide, Commission of the European Communities, Luxembourg, 1994.

Choudhury, B. J.: Radiative properties of snow for clear sky solar radiation. Computer Sciences Corporation Report., CSC/TR-79/6025: Silver Spring, Md., 1979.

Diamond, M. and Lowry, W.: Correlation of density of new snow with 700mb temperature, Research paper 1, US Army Corps of Engineers, 1953.

Dressler, K. A., Leavesley, G. H., Bales, R. C. and Fassnacht, S. R.: Evaluation of gridded snow water equivalent and satellite snow cover products for mountain basins in a hydrologic model, Hydrol. Process., 20, 673–688, 2006.

EEA: CORINE land cover technical guide – Addendum 2000, European Environment Agency, 2000.
Goudriaan, J.: Crop micrometeorology: A simulation study, Simulation monographs, Pudoc, Wageningen, 1977.
Gurtz, J., Jasper, K., and Lang, H.: Advanced flood forecasting in Alpine watershed by coupling meteorological and forecasts with a distributed hydrological model, J. Hydrol., 267, 40–52, 2002.
Henderson-Sellers, A.: Satellite sensing of a cloudy atmosphere: observing the third planet, Taylor & Francis, London and Philadelphia, 1984.
Hock, R.: Temperature index melt modelling in mountain areas, J. Hydrol, 282, 104–115, 2003.
Huwald, H., Selker, J. S., and Parlange, M. B.: Heat budget of the snow pack and interstitial exchange processes, EGU General Assembly, Vienna, Austria, 2–7 April 2006, Geophys. Res. Abstr., 8, EGU06-A-08356, 2006.
Kreider, J. F. and Kreith, F.: Solar heating and cooling: engineering, practical design, and economics, McGraw-Hill, New York, USA, 1975.
Lee, S., Klein, A., and Over, T.: A comparison of MODIS and NOHRSC snow-cover products for simulating streamflow using the snowmelt runoff model, Hydrol. Process., 19, 2951–2972, 2005.
Mancini, M.: La modellazione distribuita della risposta idrologica: effetti della variabilità spaziale e della scala di rappresentazione del fenomeno dell'assorbimento, PhD thesis, Politecnico di Milano, Milan, Italy, 1990 (in Italian).
Martinec, J.: The degree-day factor for snowmelt runoff forecasting, proceedings of general assembly of Helsinki commission on surface waters, IAHS Publ., 51, 468–477, 1960.
Martinec, J. and Rango, A.: Parameter values for snowmelt runoff modelling, J. Hydrol., 84(3–4), 197–219, 1986.
Mason, S. J. and Graham, N. E.: Conditional Probabilities, Relative Operating Characteristics, and Relative Operating Levels, Weather Forecast., 14(5), 713–725, 1999.
Metsiimiiki, S., Janne, S., Koskinen, J., and Grande, J.: The use of NOAA AVHRR imagery in snow monitoring, Geoscience and remote sensing symposium proceedings, IGRASS'98, 4, 1864–1866, doi:10.1109/IGRASS.1998.703677, 1998.
Montaldo, N., Ravazzani, G., and Mancini, M.: On the prediction of the Toce alpine basin floods with distributed hydrologic models, Hydrol. Process., 21, 608–621, 2007.
Nash, J. E., Sutcliffe, J. V.: River flow forecasting through the conceptual models, Part 1: A

discussion of principles, J. Hydrol., 10(4), 282–290, 1970.
NOAA: NOAA Polar Orbiter Data User's Guide, http://www2.ncdc.noaa.gov:80/docs/podug/index.htm, 2000.
Parajka, J. and Bloschl, G.: Spatio-temporal combination of MODIS images – potential for snow cover mapping, Water Resour. Res., 44, W03406, doi:10.1029/2007WR006204, 2008.
Rabuffetti, D., Ravazzani, G., Corbari, C. and Mancini, M.: Verification of operational Quantitative Discharge Forecast (QDF) for a regional warning system – the AMPHORE case studies in the upper Po River, Nat. Hazards Earth Syst. Sci., 8, 1–13, 2008, http://www.nat-hazards-earth-syst-sci.net/8/1/2008/.
Ranzi, R., Grossi, G., and Bacchi, B.: Ten years of monitoring areal snowpack in the Southern Alps using NOAA-AVHRR imagery, round measurements and hydrological data, Hydrol. Process., 13, 2079–2095, 1999.
Salandin, A., Rabuffetti, D., Barbero, S., Cordola, M., Volontè, G., and Mancini, M.: Il lago effimero sul ghiacciaio del Belvedere: monitoraggio e simulazione numerica del fenomeno finalizzata alla previsione e gestione dell'emergenza, Neve e Valanghe, 51, 58–65, 2004.
Shamir, E. and Georgakakos, K. P.: Distributed snow accumulation and ablation modelling in the American River basin, Adv. Water Resour., 29, 558–570, 2006.
Simpson, J. J., Stitt, J. R. and Sienko, M.: Improved estimates of the areal extent of snow cover from AVHRR data, J. Hydrol., 204, 1–23, 1998.
Tarboton, D. G., Chowdhury, T. G., and Jackson Thomas, H.: A Spatially Distributed Energy Balance Snowmelt Model, Utah Water Research Laboratory, 1994.
Tarboton, D. G. and Luce, C. H.: Utah energy balance snow accumulation and melt model (UEB), computer model technical description and users guide, Utah Water Research Laboratory, Logan, 1996.
Tachner, S., Strasser, U., and Mauser, W.: Application of remote sensing derived from NOAA-AVHRR images for spatial snow water equivalent modelling, Geoscience and Remote sensing Symposium Proceedings, IGRASS'98, 4, 1861–1863, doi:10.1109/IGRASS.1998.703676, 1998.
US Army Corps of Engineers: Snow Hydrology, US Army Corps of Engineers, Portland, OR, 1956.
USDA: U.S. Department of Agriculture, Soil Conservation Service, National Engineering Handbook, section 4, Hydrology, Rev. ed., U.S. Department of Agriculture, Washington D.C., USA, 1986.

Verbunt, M., Gurtz, J., Jasper, K., Lang, H., Warmerdam, P., and Zappa, M.: The hydrological role of snow and glaciers in alpine river basins and their distributed modelling, J. Hydrol., 282, 36–55, 2003.

Voigt, S., Koch, M., and Baumgartner, M. F.: A multichannel threshold technique for NOAA AVHRR data to monitor the extent of snow cover in the Swiss Alps. Interactions between the cryosphere and creenhouse, Procceedings of IUGG 99 Symposium HS2, Birmingham, IAHS Publ., 256, 35–43, 1999.

Table 1. Percentage of snow covered pixels from row satellite images and after elevation correction and for simulated maps with different air temperature thresholds of snow accumulation.

	satellite	satellite with correction	snow temperature thresholds (−3, 0)	snow temperature thresholds (−5, −2)	snow temperature thresholds (0, 0)	snow temperature thresholds (−1, 3)	snow temperature thresholds (1, 7)
26 September 2000	4.6	4.6	4.6	0.9	5.6	8.3	9.7
5 December 2000	45.4	69.0	55.1	43.5	60.6	62.5	71.3
10 February 2001	56.5	76.4	63.9	54.2	67.6	83.3	86.1
5 March 2001	67.6	84.3	66.2	60.2	66.2	67.1	76.4
23 March 2001	93.1	93.1	50.5	35.2	50.9	52.8	55.6
1 April 2001	49.5	53.7	48.1	32.4	48.6	49.5	53.2
19 May 2001	32.4	45.4	25.5	18.1	26.9	27.8	35.6
17 October 2001	4.2	4.2	3.7	1.4	4.2	6.5	6.9
10 November 2001	4.2	4.2	4.6	3.2	6.9	7.4	7.9
8 December 2001	0.0	11.6	15.7	11.1	16.2	26.9	27.8
3 January 2002	5.6	28.2	59.3	53.2	62.0	62.5	62.5
2 February 2002	4.6	16.2	20.4	17.6	21.3	22.7	23.1
4 March 2002	67.6	77.8	62.5	51.9	64.8	66.7	72.7
1 April 2002	11.6	11.6	25.0	22.7	25.0	29.2	30.6
11 June 2002	24.1	24.1	9.3	7.9	12.5	13.9	65.7
1 October 2002	1.9	1.9	2.3	0.5	3.7	4.2	6.9
2 November 2002	21.3	33.8	8.3	5.1	9.7	12.5	13.9
1 December 2002	45.8	52.3	46.3	35.2	54.6	61.1	77.3
3 January 2003	43.5	48.1	45.8	39.4	51.9	60.2	65.3
11 February 2003	31.0	45.4	68.1	67.1	69.9	70.8	73.1
7 March 2003	67.6	52.3	47.7	33.8	48.6	56.5	62.5
5 April 2003	35.2	49.1	30.1	18.5	34.3	35.6	44.4
24 April 2003	36.1	39.8	25.9	17.1	28.2	29.6	34.7

Table 2. Numerical criteria for the calibration of the parameters T_{low} and T_{up} of the snow accumulation model. Nash and Sutcliffe efficiency, η, and root mean square error, RMSE, are reported for both the set of not corrected classified images and corrected ones.

	Not corrected images		Corrected images	
$T_{low} \div T_{up}$	η	RMSE (pixels)	η	RMSE (pixels)
0÷0	0.510	44	0.713	36
−1÷3	0.414	48	0.707	38
−3÷0	0.542	42	0.697	37
1÷7	0.256	55	0.647	41
−5÷−2	0.439	47	0.468	50
−4÷−1	0.474	46	0.568	45

HESSD
5, 3129–3156, 2008

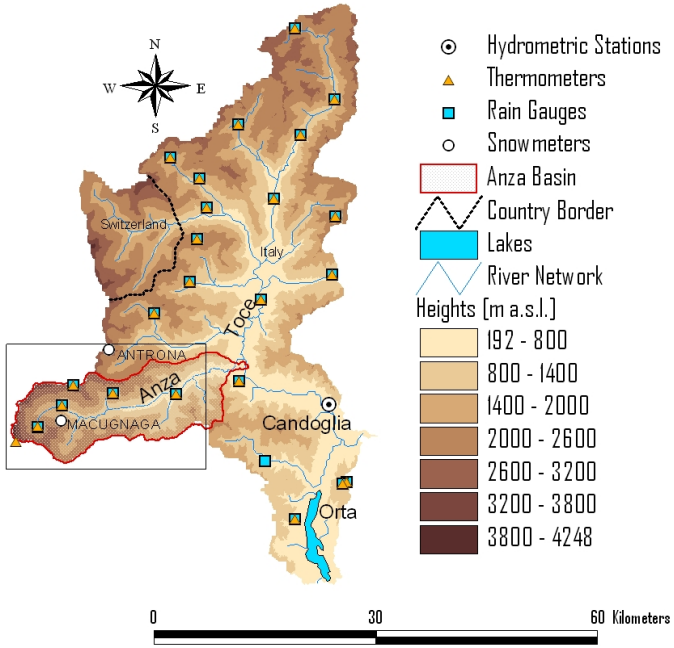

Fig. 1. The Toce watershed extracted from the digital elevation model showing locations of the rain gauges, thermometers for air temperature measurements and hydrometric stations. Red rectangle encloses the area shown in Fig. 4.

HESSD

5, 3129–3156, 2008

Snow dynamic model calibrated with satellite images

C. Corbari et al.

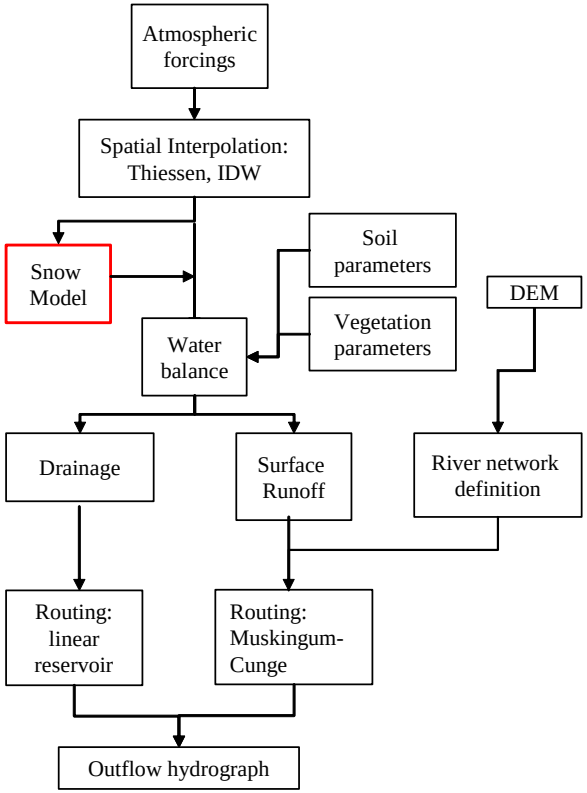

Fig. 2. Scheme of the hydrological model.

HESSD
5, 3129–3156, 2008

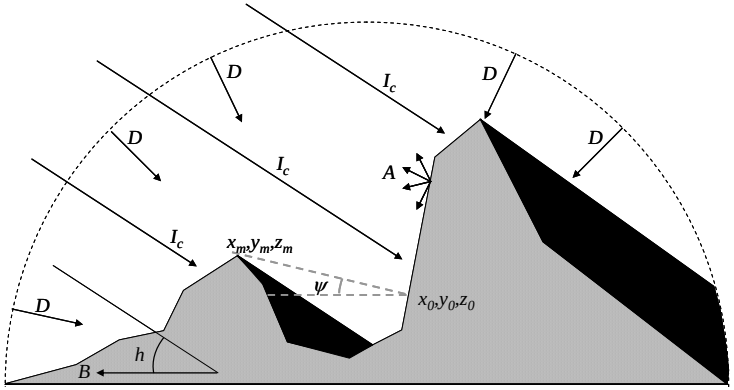

Fig. 3. Incident short wave radiation components in mountain regions for clear sky condition: direct, I_c, scattered, D and reflected from neighbour terrain, A.

HESSD

5, 3129–3156, 2008

Snow dynamic model calibrated with satellite images

C. Corbari et al.

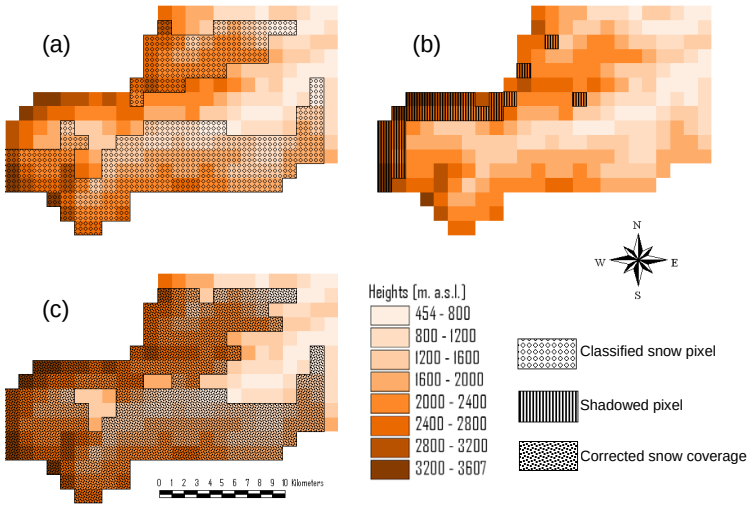

Fig. 4. Maps of the pixels classified as snow covered **(a)**, higher crests induced shadowed pixels **(b)** and resulting snow coverage after elevation based correction **(c)**. Maps are related to the 10 February 2001 NOAA-AVHRR image.

HESSD
5, 3129–3156, 2008

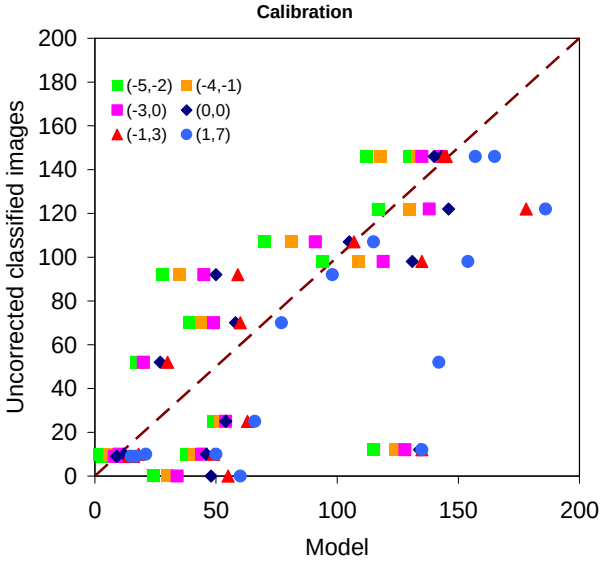

Fig. 5. Results of the calibration based on raw satellite images. The number of snow covered pixels retrieved from satellite images is plotted against the number of snow covered pixels simulated by the distributed model for five combination of T_{low} and T_{up}: $T_{low}=-1$ and $T_{up}=3$, $T_{low}=T_{up}=0$, $T_{low}=-4$ and $T_{up}=-1$, $T_{low}=-3$ and $T_{up}=0$, $T_{low}=-5$ and $T_{up}=-2$, $T_{low}=1$ and $T_{up}=7$. Every point is related to a given date and time. Linear regression and best fit line (dashed) is reported.

HESSD
5, 3129–3156, 2008

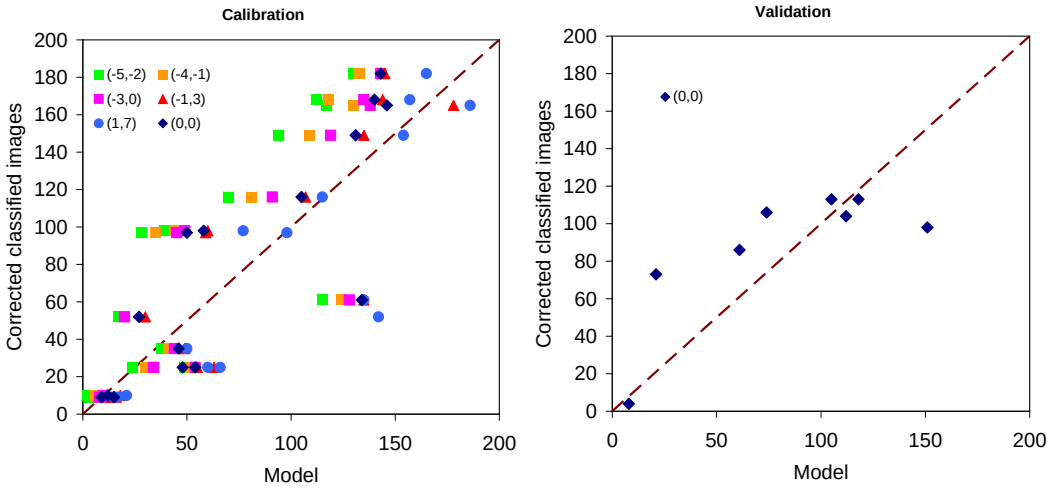

Fig. 6. Results of the calibration and of the validation based on corrected satellite images. The number of snow covered pixels retrieved from satellite images is plotted against the number of snow covered pixels simulated by the distributed model for five combination of T_{low} and T_{up}: $T_{low}=-1$ and $T_{up}=3$, $T_{low}=T_{up}=0$, $T_{low}=-4$ and $T_{up}=-1$, $T_{low}=-3$ and $T_{up}=0$, $T_{low}=-5$ and $T_{up}=-2$, $T_{low}=1$ and $T_{up}=7$. Every point is related to a given date and time. Linear regression and best fit line (dashed) is reported.

HESSD
5, 3129–3156, 2008

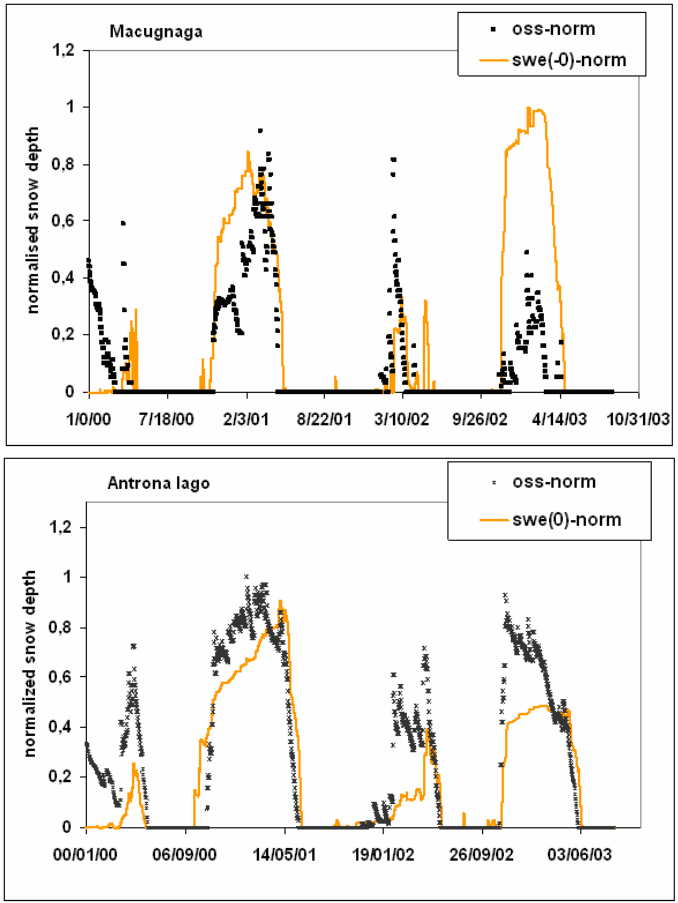

Fig. 7. Snow heights measured at Macugnaga station and Antrona Lago station compared to simulated snow water equivalent for the calibrated temperature thresholds T_{low}=T_{up}=0. Values are normalized dividing by their maximum value respectively.

HESSD
5, 3129–3156, 2008

Macugnaga station

Simulated (-3,0)

observed

	No snow	Snow
No snow	789	191
Snow	47	433

Simulated (-1,3)

	No snow	Snow
No snow	770	209
Snow	37	443

Simulated (-5,-2)

	No snow	Snow
No snow	882	98
Snow	115	365

Simulated (0,0)

observed

	No snow	Snow
No snow	817	162
Snow	40	440

Simulated (1,7)

	No snow	Snow
No snow	700	280
Snow	35	445

Antrona station

Simulated (-3,0)

observed

	No snow	Snow
No snow	469	144
Snow	21	824

Simulated (-1,3)

	No snow	Snow
No snow	444	169
Snow	18	827

Simulated (-5,-2)

	No snow	Snow
No snow	548	65
Snow	111	734

Simulated (0,0)

observed

	No snow	Snow
No snow	475	138
Snow	22	823

Simulated (1,7)

	No snow	Snow
No snow	389	224
Snow	18	827

Fig. 8. Contingency tables of binary comparison between normalized measured and simulated result in Macugnaga and in Antrona Lago stations for different values of T_{low} and T_{up}(in brackets). Results are expressed in days.

HESSD

5, 3129–3156, 2008

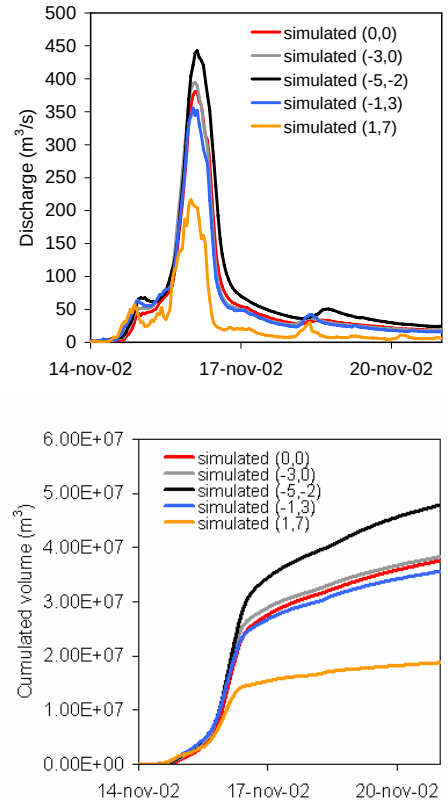

Fig. 9. The role of the temperature thresholds at the control section of Piedimulera on the simulated discharges and on the cumulated volumes.

HESSD
5, 3129–3156, 2008

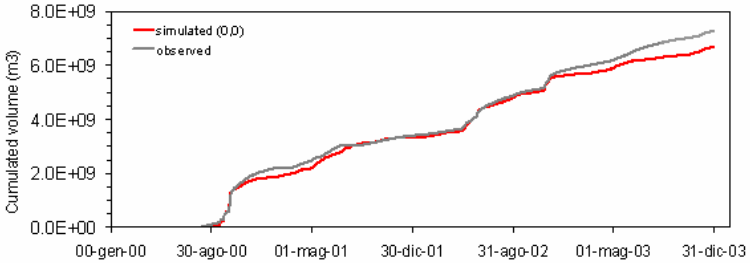

Fig. 10. Comparison between the observed and the simulated runoff volume (m^3) with the selected temperature threshold (T_{low}=T_{up}=0) at Candoglia river cross section.

HESSD
5, 3129–3156, 2008